JOURNAL OF NEUROTRAUMA 30:1512–1520 (September 1, 2013)
© Mary Ann Liebert, Inc.
DOI: 10.1089/neu.2012.2788

Long-Term *In Vivo* Imaging of Viscoelastic Properties of the Mouse Brain after Controlled Cortical Impact

Thomas Boulet,[1] Matthew L. Kelso,[2] and Shadi F. Othman[3]

Abstract

Traumatic brain injury (TBI) presents a variety of causes and symptoms, thus making the development of reliable diagnostic methods and therapeutic treatments challenging. Magnetic resonance elastography (MRE) is a technique that allows for a noninvasive assessment of the mechanical properties of soft biological tissue, such as tissue stiffness, storage modulus, and loss modulus. Importantly, by quantifying the changes in the stiffness of tissue that is often associated with disease, MRE is able to detect tissue pathologies at early stages. Recent improvements in instrumentation have allowed for the investigation of small samples with microscopic resolution (μMRE). We hypothesize that μMRE can sensitively detect variations in micromechanical properties in the brain caused by the compressive and shearing forces sustained during TBI. To test this hypothesis, we randomized 13 C57BL mice to receive a controlled cortical impact at a 0.5 mm or 0.75 mm depth, with both sham and naïve mice as controls. Our objective was to propagate mechanical shear waves throughout the brain for *in vivo* TBI μMRE imaging. The mechanical properties of the injured brain tissue were determined at days 0, 1, 7, and 28 post-injury. For both groups, we observed a significant drop in the stiffness of the impacted region immediately following the injury; the 0.75 mm animals experienced increased tissue softness that lasted longer than that for the 0.5 mm group. Although the shear stiffness, storage modulus, and loss modulus parameters all followed the same trend, the tissue stiffness yielded the most statistically significant results. Overall, this article introduces a transformative technique for mechanically mapping the brain and detecting brain diseases and injury.

Key words: inverse problem; MRE; MRI; TBI; viscoelasticity

Introduction

Traumatic brain injury (TBI) is a diverse and complex injury affecting 1,700,000 Americans annually.[1] Although most people with TBI survive the injury, they often have permanent cognitive loss, behavioral issues, and emotional disturbances.[2] The mechanisms responsible for these functional losses remain unclear. Additionally, the behavioral effects of TBI remain difficult to predict, given that similar injuries can induce diverse symptoms.

Magnetic resonance imaging (MRI) techniques, which utilize different mechanisms to provide a visual contrast between tissues, significantly contribute to understanding TBI. For example, T2-weighted imaging, a type of MRI utilizing relaxation time, has been shown to be effective in imaging edema. Similarly, T2-weigted imaging has revealed areas of T2 hypointensity in both the thalamus and internal capsule of the brain after inducing TBI in mice in the laboratory.[3,4] Another type of MRI is diffusion tensor imaging, which measures microstructural tissue abnormalities that correlate pathologically with damaged white and gray matter. Furthermore, the diffusion tensor technique has shown reduced axial diffusivity and relative anisotropy in animal models of TBI.[5] Alternatively, iron oxide-enhanced MRI and arterial spin-labeling MRI have been used to monitor cerebral blood flow following TBI in mice by measuring changes in T1 relaxation times between selective and nonselective scans.[6,7]

A clinical MRI technique called magnetic resonance elastography (MRE) was developed to gauge the mechanical tissue stiffness of whole organs with MR spatial resolution (e.g., 1 mm × 1 mm × 5 mm). Mechanical stiffness is well known to be important for load-bearing tissues such as the musculoskeletal structures, but mechanical stiffness has also been shown to be an indicator of the structural health of non-load-bearing tissues such as neural, dermal, and vascular tissues.[8,9] As a diagnostic tool, MRE combined with proper excitation methods allows for quantitative and noninvasive palpation of remote soft tissues in the body. To accomplish this, MRE measures motions in soft biological tissues induced by the vibrations of a mechanical actuator. In turn, algorithms are applied to the motions induced by the vibrations in order to estimate local values of the mechanical properties of the tissue.[10] Importantly, MRE is able to detect tissue pathology stages earlier

[1]Department of Engineering Mechanics, and [3]Department of Biological Systems Engineering, University of Nebraska-Lincoln, Lincoln, Nebraksa.
[2]Department of Pharmacy Practice, College of Pharmacy, University of Nebraska Medical Center, Omaha, Nebraska.

than conventional MRI, ultrasound, or X-ray/computed tomography (CT), and is currently used to study the pathologies of various organs, including the liver in patients with hepatic fibrosis.[11,12]

Continuous advancements have been made in MR hardware to improve the sensitivity and resolution of images. These hardware improvements include stronger magnets and gradients, and more sensitive radiofrequency (RF) imaging coils. Such advancements allow for the investigation of small samples with microscopic resolution. This has been accomplished through the creation of a technique termed microscopic MRE, or μMRE.[13,14]

We hypothesize that μMRE can detect subtle variations in micromechanical properties of tissues caused by the compressive and shearing forces sustained by the brain during TBI. Thus, information provided on the micromechanical properties of the brain after TBI is expected to help evaluate the health of brain tissue. Previously, we tested this hypothesis using a rat model in which the brain had been excised following controlled cortical impact (CCI) over a 28-day period. The mechanical properties represented by stiffness — a parameter equivalent to the elastic shear modulus — were estimated at 370 Hz. The stiffness of the somatosensory cortex of the impacted hemisphere decreased by 25% following TBI.[15] Such strong results prompted an *in vivo* study.

Performing μMRE of the brain *in vivo* is challenging, given that it is necessary to propagate mechanical waves through the skull. In the study discussed herein, the μMRE technique was used after CCI was administered to a live mouse brain at different impact depths (0.5 mm and 0.75 mm). In the present study's design, a vibrating bite bar setup was designed for the μMRE to propagate sinusoidal shear waves at 877.5 Hz from a piezoelectric bending element into the mouse brain. The displacement field created by these cyclic perturbations was then captured using a phase-contrast MR imaging pulse sequence and analyzed by a direct inversion algorithm to estimate local values of viscoelastic properties in different regions of interest (ROIs). The experimental design is further described in Figure 1.

Methods

Animal handling

This study utilized 13 C57BL/6 adult male mice (Jackson Laboratory, Bar Harbor, ME). The animals were housed in individual cages in a climate-controlled room and kept on a 12 h light/dark cycle. Continual access to food and water was provided throughout the duration of the study. All procedures and protocols were approved by the Institutional Animal Care and Use Committee of the University of Nebraska-Lincoln and conducted in accordance with the National Institutes of Health Guide for the Care and Use of Laboratory Animals.

All mice were 3 months old at the start of the study. The mice were selected at random to be exposed to CCI injury, sham injury, and no injury, as previously described.[16,17] Following the induction of anesthesia with 5% inhaled isoflurane, the heads of the mice were shaved and positioned in a Kopf stereotaxic head frame (David Kopf Instruments, Tujunga, CA). Anesthesia was maintained with 2% inhaled isoflurane, which was delivered through a

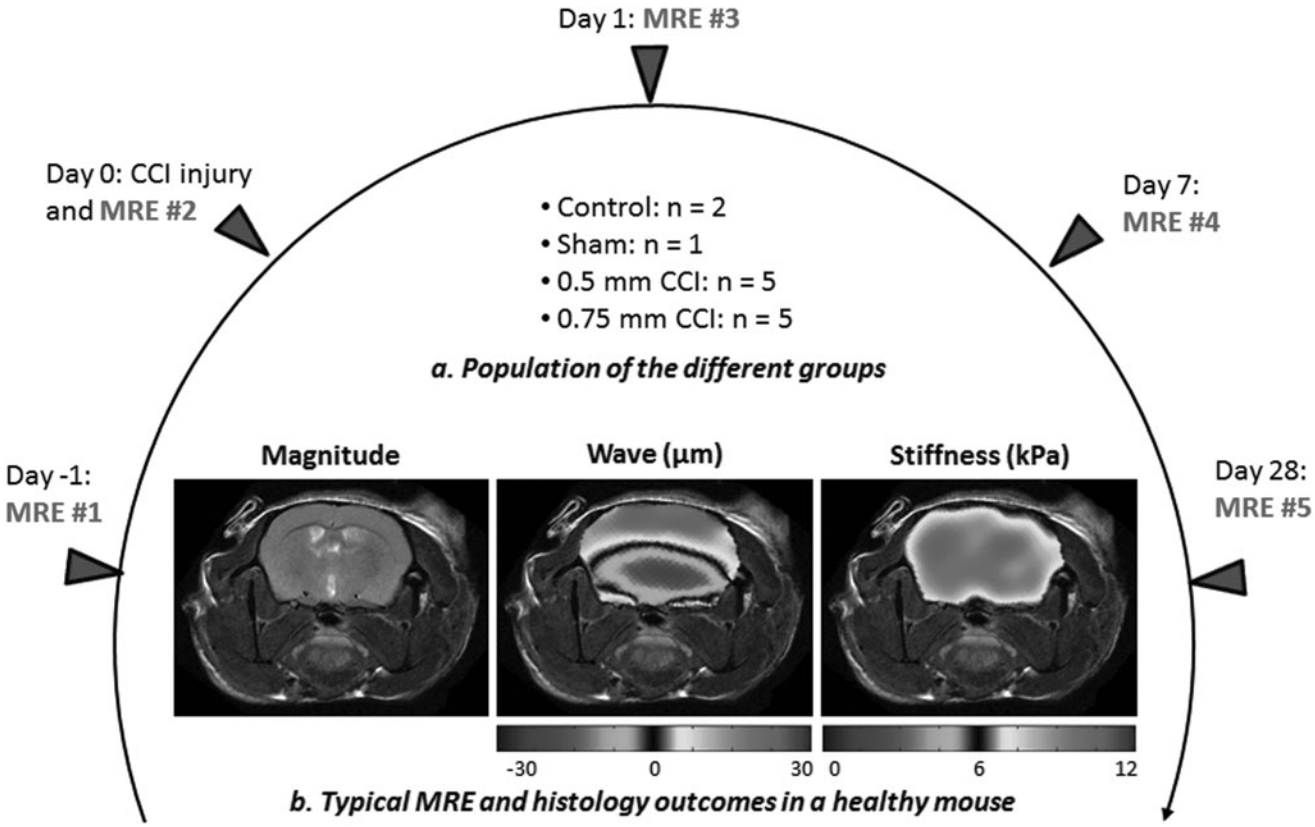

FIG. 1. Timetable of the magnetic resonance elastography (MRE) experiments used for each mouse in the study. MRE was performed at five different time points within a 29 day time frame. **(a)** Animals were divided into different groups: 0.75 mm controlled cortical impact (CCI) injury, 0.5 mm CCI injury, craniotomy without injury (sham), and naive. **(b)** Typical MRE experiment performed at 900 Hz on a healthy mouse brain.

nose cone. A midline incision was completed, and a 4 mm craniotomy was performed lateral to the midline and midway between bregma and lambda to expose the underlying somatosensory cortex, taking care not to disturb the dura. The head frame was then positioned beneath a Precision Systems and Instrumentation TBI-0310 (Fairfax Station, VA) that administered a 0.5 mm or a 0.75 mm cortical compression (3 mm impactor diameter, 3.5 m/sec velocity, 500 msec dwell time). Following injury, Surgicel (Johnson & Johnson, Dallas, TX) was placed over the injury site. Next, the skull cap was put back in place and sealed using dental acrylic. The skin incision was closed with sutures, and the incision was infused with 0.5% bupivacaine with 1:200000 epinephrine as a topical analgesia. Conversely, animals receiving a sham injury underwent an identical surgical procedure, with the exception of the impact. Control animals were left intact. Following closure, the animals were placed in their home cage and imaged on 0, 1, 7, and 28 days post-injury.

MRI system and μMRE parameters

MR experiments were conducted at 9.4 T (400 MHz for protons) using an 89 mm vertical bore magnet (Agilent Technologies, Santa Clara, CA). MRE measurements were acquired using a 4 cm Millipede RF imaging probe with triple axis gradients (maximum strength 100 G/cm).

A custom-phase, contrast-based μMRE pulse sequence was integrated into the VnmrJ 2.3A imaging software. The pulse sequence enables the user to select parameters such as the gradient amplitude, actuator frequency, delay between the mechanical actuator and the bipolar gradient, motion sensitizing gradient direction, and number of bipolar pairs. The μMRE system was designed so that the modified pulse sequence controls the oscillator, which is synchronized to the motion sensitizing gradient. The design and implementation of this system has been previously described.[14]

The μMRE experiments were conducted using a gradient echo-based phase contrast sequence, which offers improved signal-to-noise ratio compared with a spin echo-based sequence. The following parameters were used: repetition time (TR) = 1 sec, echo time (TE) = 6 ms, field of view (FOV) = 20 mm × 20 mm, slice thickness = 1 mm, matrix dimension = 128 × 128, mechanical frequency = 877.5 Hz, gradient amplitude = 100 G/cm, number of excitations (NEX) = 2, motion sensitizing gradient direction = slice, number of bipolar pairs = 3, and total acquisition time per animal $\approx$ 2 h.

Experimental design

Of the 13 animals used in this study, the procedures were divided among them into the following four categories: 1) five mice were subjected to a 0.5 mm depth CCI; 2) five mice were subjected to a 0.75 mm depth CCI, 3) one mouse underwent a craniotomy without injury (sham), and 4) two mice were left intact (control). Anesthesia was maintained with 1.5–2% inhaled isoflurane throughout all imaging experiments, and respiration rate was continually monitored (Small Animal Instruments, Inc., Stony Brook, NY). The body temperature was traced using a temperature probe and automatically adjusted by a controller unit via an air heater.

The propagation of mechanical shear waves throughout the brain is required for *in vivo* μMRE imaging of a mouse brain. To achieve this, an animal holder featuring a vibrating bite bar was designed (Fig. 2). After being placed under anesthesia (2% inhaled isoflurane) in a closed chamber, the top front teeth of the mouse were placed in a hole at the end of the bite bar, which was then pulled back to position the head of the mouse into a nose cone delivering the isoflurane/oxygen mixture. The shape of the nose cone ensured that the animal's jaw remained closed, thus securing the jaw and the bite bar. An L-shaped connector was utilized to bind the other end of the bite bar to a piezoelectric bending element transducer (model T234-H4CL-303X, Piezo system, Woburn, MA). The bite bar was made of copper in order to be rigid enough to propagate the vibrations from the actuator through the mouse head, while at the same time being nonmagnetic to avoid creating artifacts. The actuator was driven by a signal generator (Tektronix, Beaverton, OR) followed by an amplifier (Piezo system, Woburn, MA), delivering a 200 V signal.

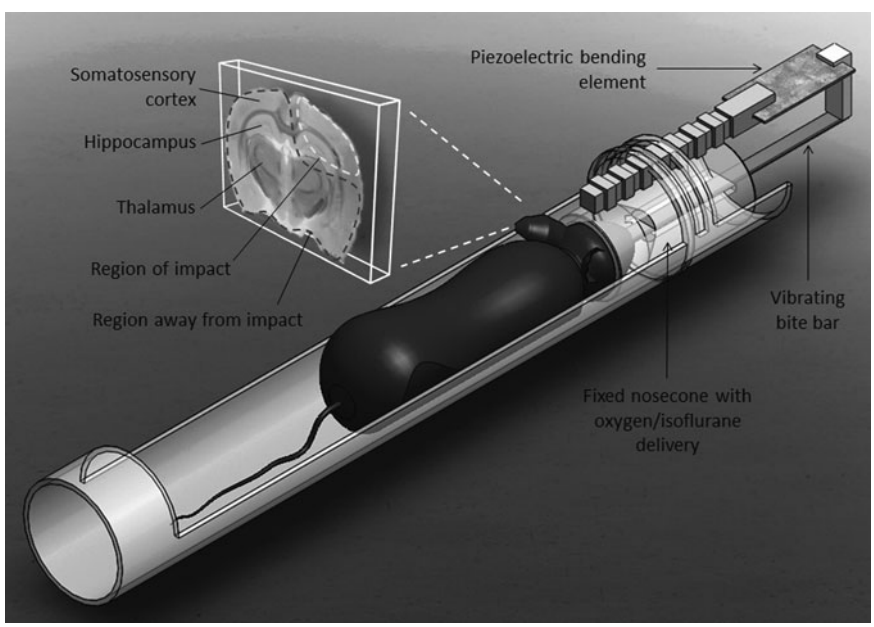

FIG. 2. Experimental setup for conducting *in vivo* experiments. For imaging, a coronal slice including the injury site was selected, exposing regions such as the somatosensory cortex, the hippocampus, and the thalamus. Regions for which results were reported are defined as the region of impact (surrounded by dotted line at upper right, consisting of the somatosensory cortex and part of the hippocampus of the injured hemisphere) and the region away from impact (surrounded by dotted line, consisting of the rest of the brain). These two regions of interest (ROIs) were selected for every mouse, whether it was injured or not.

After the mouse was properly connected to the bite bar, the mechanical vibrations of the system were characterized using a laser Doppler vibrometer (Polytec, Dexter, MI). The vibrometer was able to measure the oscillations of the bite bar by pointing a laser beam on its surface and analyzing the reflected signal. The goal of this procedure was to identify the resonance frequencies, in order to conduct experiments at these specific frequencies, and, hence, optimize the amplitude of the generated waves. The transducer behavior was first characterized by sending a white noise (signal composed by all frequencies in the 10 Hz–2 kHz range) from the signal generator to the actuator and recording the measured displacement.

The spectrum of this measured displacement was computed to reveal the resonance frequencies of the system, which are the frequencies for which the output displacement is magnified. A signal generator was then used to deliver signals at these specific frequencies, and the output displacement was measured. It is important to note that we did not observe any damage to the teeth as a result of this procedure over the 1 month study. For imaging purposes, a slice was selected to be imaged in the coronal plane, approximately halfway through the brain, to include the injury site/ROI, as well as the region outside the ROI (outside ROI) that included the rest of the somatosensory cortex, hippocampus, and thalamus of both hemispheres (Fig. 2). Areas for similar regions were selected as ROIs for the control mice.

An experiment was conducted on a 1% wt agarose gel phantom to investigate the range of frequencies provided using our instrumentation. This range is presented in Figure 3, where displacement maps are displayed at 400 Hz and 1 kHz. At such high frequencies, wavelengths become much shorter, thus improving the accuracy of the estimated mechanical properties. Using the described setup, the amplitude of vibrations reached $\sim 300\,\mu$m at 877.5 Hz, and, therefore, this was the frequency selected for this study.

Inversion algorithm

To calculate local values of the mechanical properties of tissues from the measured displacement field, we utilized a custom-written algorithm based on a previously developed spatiotemporal filtering approach,[18–20] which has been thoroughly described in an earlier study.[15] This algorithm can be executed in < 1 min using a conventional desktop to calculate the mechanical properties.

The algorithm assumed planar shear waves propagation in isotropic and unbounded media. A linear viscoelastic material model was selected, and a multidirectional filter was used to identify waves propagating at a single frequency and in specific directions. Mechanical properties were averaged from data sets that were filtered in eight different directions in order to improve the faithfulness of the recovery of data when studying complex wave patterns. The algorithm also allowed for the selection of the ROI. For each region, the mean and standard deviation were calculated for each parameter. The parameters included, as defined subsequently, the storage (G') and loss (G'') moduli, which are the real and imaginary parts of the complex-valued shear modulus, as well as the overall shear stiffness μ:

$$\mu(\mathbf{a},f) = \rho(\mathbf{a})c_s(\mathbf{a},f)^2 \tag{1}$$

In this equation, a is the position, f is the frequency; ρ is the density of the material (assumed to be uniformly 1,000 kg/m^3); and c_s is the speed of a hypothetical plane-wave propagating through an infinite medium composed of the same material.

Statistical analysis

The selection of the ROI was based on the location of the impact as seen on MR images, as well as on stiffness maps.

The severity of each injury was analyzed using a two way analysis, repeated measures of variance (ANOVA) to determine the change in tissue stiffness, storage moduli, and loss moduli between the ROI and the region outside the ROI over the 28 day study. A Bonferroni procedure was used for *post-hoc* comparisons. The data were analyzed using GraphPad Prism 5 (La Jolla, CA). The significance was defined as $\alpha = 0.05$. All data are presented as mean ± standard deviation.

Results

Estimations of tissue stiffness, in addition to storage and loss moduli, for each injury severity at different time points (before injury, immediate, 24 h, 7 days, and 28 days) are presented in Table 1. For the immediate measurements, all mice were imaged within 6 h of injury. Values of stiffness for the sham and control mice were consistently $\sim$ 9 kPa in every ROI at each time point. More specifically,

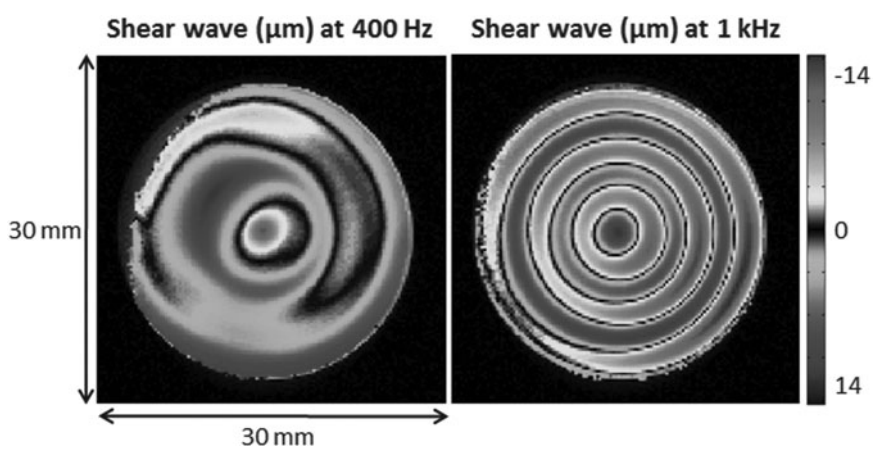

FIG. 3. Shear waves measured at 400 Hz and 1 kHz in a 1% wt agarose gel. The MR sequence used was a gradient echo based elastography sequence with the following imaging parameters: repetition time (TR) = 1 sec, echo time (TE) = 8 ms at 400 Hz and 5.6 ms at 1 kHz, field of view (FOV) = 30 mm × 30 mm, slice thickness = 1 mm, matrix dimension = 128 × 128 pixels, number of excitations (NEX) = 2, gradient amplitude = 100 G/cm, and number of bipolar pairs = two at 400 Hz and three at 1 kHz. This demonstrates the feasibility of propagating measurable shear waves at frequencies up to 1 kHz where wavelengths are much smaller, thus improving the faithfulness of the recovery.

Table 1. Mean Values of Mechanical Parameters Estimated at 877.5 Hz for Each Injury Severity in Different Regions of the Brain and at Different Time Points following the Injury

			Before injury	*Immediate*	*24 h*	*7 days*	*28 days*
TBI 0.5 mm ($n=5$)	Region of impact	Stiffness (kPa)	9.0	7.1	7.5	8.8	9.0
		Storage modulus (kPa)	5.6	4.1	4.7	5.7	5.5
		Loss modulus (kPa)	4.5	3.6	3.8	4.4	4.5
	Away from impact	Stiffness (kPa)	9.0	9.3	9.7	9.6	9.3
		Storage modulus (kPa)	5.8	5.8	6.4	6.2	5.8
		Loss modulus (kPa)	4.4	4.7	4.7	4.6	4.6
TBI 0.75 mm ($n=5$)	Region of impact	Stiffness (kPa)	9.4	6.8	7.9	8.2	8.9
		Storage modulus (kPa)	5.8	4.1	5.0	5.1	5.3
		Loss modulus (kPa)	4.6	3.4	4.0	4.1	4.6
	Away from impact	Stiffness (kPa)	9.5	9.5	10.2	10.0	9.6
		Storage modulus (kPa)	6.2	5.9	6.6	6.6	6.1
		Loss modulus (kPa)	4.6	4.7	5.0	4.9	4.7

The standard deviation values, not depicted here, were all ranging from 10% to 22%.
TBI, traumatic brain injury.

values of stiffness, storage modulus, and loss modulus averaged 9.2 ± 1.1 kPa, 5.7 ± 0.9 kPa, and 4.5 ± 0.6 kPa, respectively, for the sham and control mice over each time point.

Representative images of a mouse subjected to a CCI injury at a 0.75 mm indentation depth are shown in Figure 4. In the magnitude image, one of the eight shear waves resulting from the directional filtering and the estimated stiffness are displayed for each time point; the injury site is highlighted. It is clear from these data that the impacted region experienced a decrease in stiffness immediately following TBI compared with statistically insignificant changes in the rest of the brain. The waves measured in the brain had amplitudes of $\sim 40\,\mu$m, which allowed for motion to register with an appropriate signal-to-noise ratio. Furthermore, the softening of the brain observed in the stiffness maps was confirmed by a shorter wavelength in the region of impact following injury. This phenomenon is particularly noticeable in the shear wave image of the 24 h time point, as shown in Figure 4.

Immediately following injury, the stiffness in the ROI decreased $\sim 24\%$ in the 0.5 mm group and 29% in the 0.75 mm group compared with the area outside the ROI (Fig. 5). By day 7, the stiffness in the ROI of the 0.5 mm group had recovered to near control levels, whereas the ROI of animals impacted by a 0.75 mm hit was still $\sim 18\%$ less stiff than the rest of the brain. Statistical analysis found a significant interaction between region and time for both the 0.5 mm and 0.75 mm groups ($F[4,32] = 4.84$, $p < 0.01$ and $F[4,32] = 5.13$, $p < 0.01$, respectively). Bonferroni *post-hoc* analysis confirmed that the stiffness of the ROI significantly decreased compared with the rest of the brain immediately following injury for both groups, and recovered by 7 days for the 0.5 mm group and by 28 days for the 0.75 mm group. A similar finding was observed for the loss moduli in both groups, with decreases of $\sim 23\%$ and 28% immediately following injury for the 0.5 mm and 0.75 mm groups, respectively. As with the stiffness measurements, by day 7, the loss moduli had recovered for the 0.5 mm group, whereas the loss moduli for 0.75 mm group still decreased by 15%. The storage moduli measurement appeared to be a less sensitive measure than either the stiffness or loss moduli. Immediately following injury, there was a 28% decrease in the storage moduli at the ROI of animals injured with a 0.5 mm injury versus a 30% decrease in the storage moduli for the 0.75 mm group. Although the storage moduli for the ROI in the 0.75 mm group still decreased by $\sim 13\%$ at 28 days, it was not significant. Statistical analyses revealed a significant interaction between the two terms ($F[4,32] = 3.32$, $p < 0.05$) for the 0.75 mm group. However, the interaction was not significant for the 0.5 mm group, although the main effect of the region ($F[1,8] = 29.77$, $p < 0.001$) and recovery time ($F[4,32] = 2.77$, $p < 0.05$] did achieve significance.

Discussion

The mechanical properties of brain tissue, as measured *in vivo* using the μMRE technique, were found to be affected by TBI in mice. More specifically, a major decrease in the shear stiffness of the impacted region occurred immediately following injury. This was found to be the result of a combined decrease of both storage moduli and loss moduli. The extent and significance of this drop increased with the injury severity. The most statistically significant results occurred in the somatosensory cortex and part of the hippocampus within 24 h after TBI. Still, some differences were still observed after 1 week, particularly in the case of an injury at an indentation depth of 0.75 mm. No difference was observed between the sham and the control group, indicating that craniotomy alone does not affect brain mechanical properties.

This study demonstrated the potential of μMRE to improve diagnosis of TBI by noninvasively assessing brain viscoelastic properties. Periodic monitoring of mice allowed us to obtain statistically significant results using a relatively low number of animals. In future studies, it will be important to correlate the μMRE findings with th pathophysiology of the injury. A likely pathophysiological mechanism is the formation of edema following injury.[21] Previous work found an inverse correlation between the formation of edema and tissue stiffness following experimental ischemia and cryolesioning.[22,23] Our study revealed a decrease in the tissue stiffness of the injured brain region immediately following injury. This stiffness persisted for $\sim$ 7 days, suggesting the presence of edema. This time frame is generally accepted as the time when the damaged cerebrovasculature is most permeable and allows for the passage of water and serum proteins to the parenchyma.[24–26]

Another potential cause of the reduced tissue stiffness is the reduction in cerebral blood flow accompanying CCI. A recent study to determine the effect of blood flow on the shear stiffness of pig kidneys using MRE found that an increase in tissue stiffness correlated with a reduction in blood flow.[27] Another recent

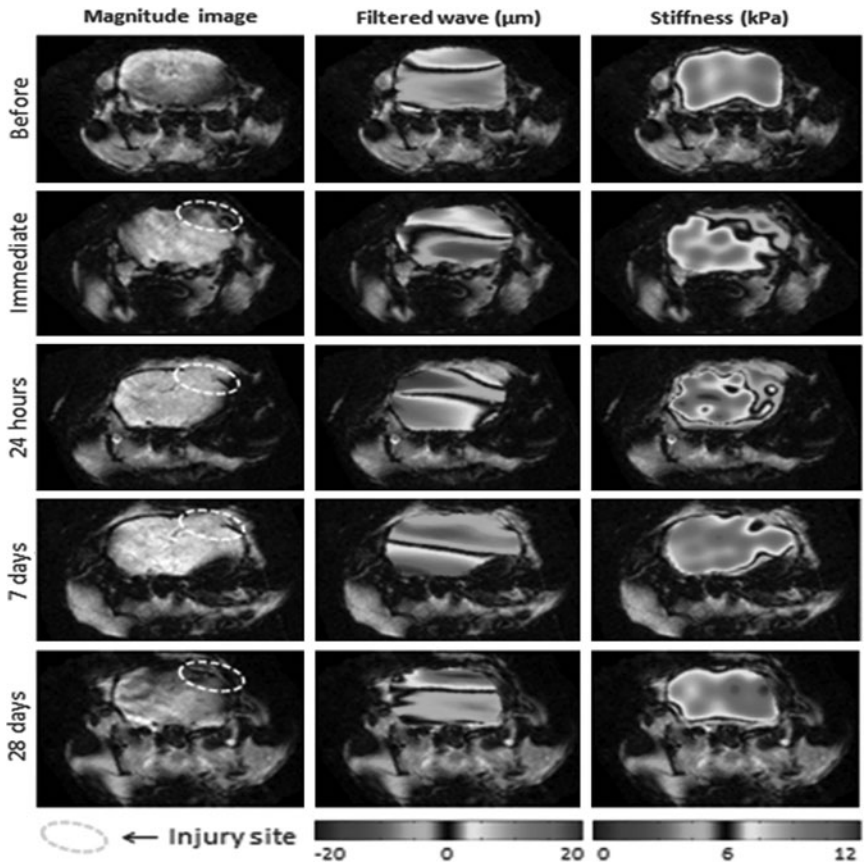

FIG. 4. Magnitude images, filtered shear wave, and stiffness estimations of a mouse brain at different time points: before injury, immediately, and 24 h, 7 days, and 28 days following controlled cortical impact (CCI) injury with a 0.75 mm indentation depth. The injury site was located on one hemisphere, highlighted on the magnitude images. This reduction pattern can also be noticed by shorter wavelength in the shear wave images in the injured regions.

study suggested that cerebral blood flow may decrease as much as 90% in the contusion area following a CCI in mice;[28] however, this decrease was not associated with expansion of the contusion volume. Interestingly, previous reports show an ~50% reduction in the cerebral blood flow throughout the brain following CCI.[28]

Additional work is necessary to determine the role of different pathologies, such as edema and cerebral blood flow, in the reduction of tissue stiffness. Future studies can correlate μMRE findings with additional MR measurements such as T2-relaxation time and diffusion tensor imaging, as well as histological markers, by euthanizing the animal immediately following imaging and attempting to correlate μMRE findings with other MR measurements and histology, which was not permitted using our experimental design. These additional studies are also expected to help determine the cause of the large variance at the early time points following injury, when hemorrhage, edema, and alterations in cerebral blood flow most likely occur.[24,25,28,29]

In our current study, the mice were injured and studied over a period of 28 days before being euthanized. Previous work has shown that following a CCI, wet-dry methods for assessing edema show that the water content in the brain returns to baseline levels at ~7 days,[24,30] as do histological markers such as horseradish peroxidase[31] and measurements of specific gravity.[25] Likewise, Aquaporin-4, a protein involved in the homeostasis of water, has recently been shown to normalize by 30 days following CCI.[32]

The values of the material parameters measured in this study are on the same order of magnitude as those reported in the literature for mice measured at similar frequencies.[33–35] Table 2 shows the results from these different studies.[33–35] In comparison to μMRE, nano-indentation and atomic force microscopy exhibited regional variations of < 100% in rat and porcine brains.[36–40] Disparities in mechanical properties from one study to another could be explained by differences in experimental protocols, such as the animal strain, age, and/or the operating frequency. Similarly, regional variations would more likely originate from low signal-to-noise ratios or from disparities in the inversion methods utilized. As pointed out by Atay et al.,[33] some regions of the brain can experience destructive wave interference and low signal-to-noise ratios, resulting in significant errors in the recovery. In highly viscoelastic materials, large wave attenuation coefficients could also be responsible for poorly resolved wave distributions. Therefore, it is critical to ensure that the shear waves are propagated with a measurable amplitude throughout the entire tissue of interest.

In this study, the operating frequency was carefully selected to maximize the amplitude of the imparted motion, as described in the Methods section. MRE experiments were performed at a resonance frequency of the mechanical system that allowed for wave propagation to occur throughout the brain. The code developed for this study featured a multidirectional, spatiotemporal filter designed to separate waves propagating in different directions, thus avoiding destructive interferences. The mechanical properties were

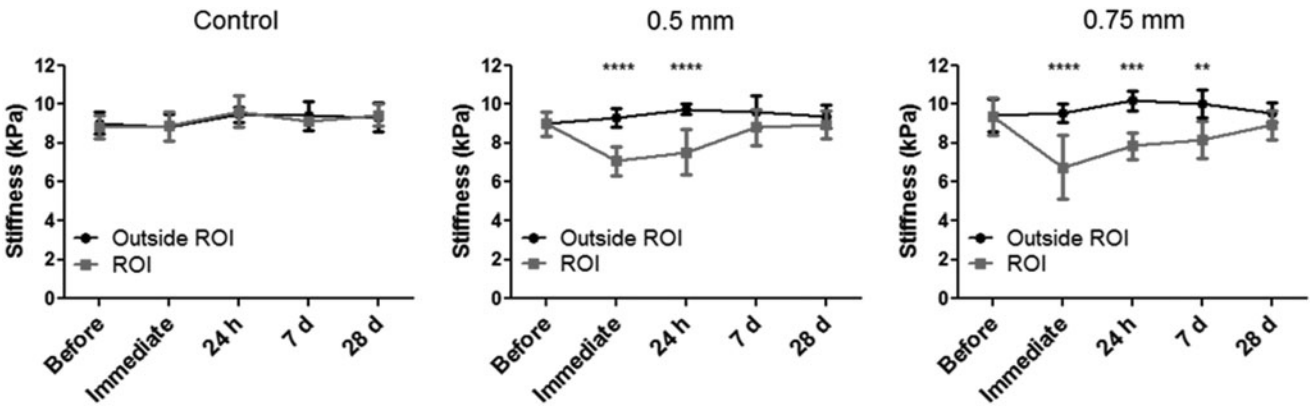

FIG. 5. Brain stiffness measured with magnetic resonance elastography (MRE) at different time points for control animals and those with each injury severity. Analysis of the graphs reveals a drop in stiffness values in the impacted region immediately following injury, while values in the rest of the brain remain unchanged. The statistical significance of this drop increases with injury severity and decreases with time as mechanical properties of the injured tissue progressively rise to match their primary values. There were no differences between the two regions of control animals. $****p<0.0001$; $***p<0.001$; $**p<0.01$. All values are reported as the mean ± standard deviation of the groups.

estimated from eight different angles of propagation (every 45 degrees) and averaged pixel by pixel, with a weight depending upon the relative intensity of each filtered data set at this location. Consequently, the properties estimated from low-amplitude waves were poorly determined, and carried a lower weight than those estimated with better accuracy, hence minimizing errors in the recovery of data.

The algorithm utilized assumes infinite media for the calculation of the mechanical properties. For imaging a small organ such as the mouse brain, this assumption can be used by increasing the operating frequency, thereby reducing the wavelength. At a higher frequency, the wavelength becomes shorter than the width of the mouse brain, thus the error generated by this assumption is reduced. The experiment presented in Figure 3 allowed us to explore the potential of μMRE at a higher frequency. The increase in operating frequencies compared with our previous study improved the accuracy of the estimates. However, the tissues imaged became smaller (mouse brain vs. rat brain), resulting in similar ratios

Table 2. Experimental Parameters and Main Outcomes of Previous MRE Studies Performed on Healthy Mouse Brains *in Vivo*

	Atay et al. 2008	*Clayton et al. 2011*	*Murphy et al. 2012*	*Present study*
Mouse strain and age	C57BL/6 12–15 weeks	BALB/c 9–10 weeks	WT (euthanized prior to imaging) 73–96 weeks	C57BL/6 12–16 weeks
MR field	11.7 T	4.7 T	3 T	9.4 T
Gradient strength	10 G/cm	60 G/cm	2.73 G/cm	100 G/cm
Spatial resolution	0.25 × 0.25 × 0.4 mm	0.25 × 0.25 × 0.25 mm	0.46 × 0.46 × 3 mm	0.15 × 0.15 × 1 mm
Actuation mechanism	Electromagnetic actuator	Amplified piezoceramic actuator	Electromechanical actuator	Piezoelectric bending actuator
Inversion algorithm	Helmholtz decomposition + elastic model	Least square fitting of a viscoelastic model	Spatio-temporal directional filtering + elastic model	Spatio-temporal directional filtering + viscoelastic model
Frequency	1200 Hz	600–1800 Hz (shown at 800 Hz)	1500 Hz	877.5 Hz
Mean properties	μ = 12.6–18.7 kPa	G' = 2–8 kPa G'' = 1–3 kPa	μ = 22–28 kPa	μ = 9.2 ± 1.1 kPa G' = 5.7 ± 0.9 kPa G'' = 4.5 ± 0.6 kPa
Typical elastogram and variations within a brain	 5 kPa < μ < 25 kPa	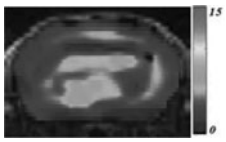 0 kPa < G' < 10 kPa	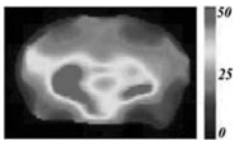 5 kPa < μ < 50 kPa	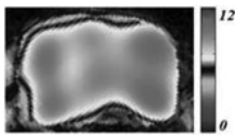 6 kPa < μ < 12 kPa

μ is the shear stiffness, G' the storage modulus, and G'' the loss modulus.
MRE, magnetic resonance elastography.
Figures reproduced with permissions of the publishers: ASME for Atay et al. 2008 (DOI: 10.1115/1.2899575), IOP for Clayton et al. 2011 (DOI: 10.1088/0031-9155/56/8/005), and Elsevier for Murphy et al. 2012 (DOI: 10.1016/j.mri.2011.12.019).

between wavelengths and the size of the samples. More powerful stack actuators and high-voltage amplifiers were implemented in the original design, generating measurable waves at frequencies up to 2.5 kHz in agarose gels, thus further reducing the wavelength and approaching the conditions of propagation in an infinite medium. However, issues of inefficient mechanical coupling and large wave attenuation prevented the implementation of such a system in mice. Solutions for delivering motion with increased amplitude are currently under investigation.

Our studies measuring the mechanical properties of brain tissue following CCI introduce a transformative method for mechanically mapping the brain. The simplicity of our design provides a pathway to clinical translation. Currently, several groups have attempted to perform MRE on human brains using fast multishot spiral readouts[41] or high field clinical scanners.[42] Both of these studies used a ~40 Hz shaker connected to the cranium. We expect that adaptation of this design can be translated to clinical settings by augmenting the waves through different acoustic windows connected to the human brain (e.g., inducing vibration in the neck to propagate waves to the brain through the carotid artery). Multiple actuators can be synchronized simultaneously to generate stronger waves at higher frequencies.

Conclusion

In conclusion, elastography imaging techniques have the potential to address the understudied area of noninvasive mechanical assessment of TBI, because of their excellent penetration depth, even in the deep brain tissue encased by the skull. We have shown the potential for μMRE to provide noninvasive *in vivo* imaging markers using an animal model, which could, in turn, be used to examine the neuropathology and pathogenesis of brain diseases in humans.

Acknowledgments

The authors thank Vahid Khalilzad-Sharghi for his technical assistance with the MRE pulse sequence, as well as the publishers and authors mentioned in Table 2 for providing their permission to replicate a figure. The authors also thank Melody Montgomery for help in editing this manuscript. This research was supported in part by University of Nebraska-Lincoln (UNL)/University of Nebraska Medical Center (UNMC) Engineering for Medicine Research Collaboration Seed Grant and National Institutes of Health (NIH) COBRE grant RR021937 (Nebraska Center for Nanomedicine).

Author Disclosure Statement

No competing financial interests exist.

References

1. Faul, M. (2010). *Traumatic Brain Injury in the United States: Emergency Department Visits, Hospitalizations and Deaths 2002–2006.* U.S. Department of Health and Human Services: Atlanta.
2. Babikian, T., and Asarnow, R. (2009). Neurocognitive outcomes and recovery after pediatric TBI: meta-analytic review of the literature. Neuropsychology 23, 283–296.
3. Tsenter, J., Beni-Adani, L., Assaf, Y., Alexandrovich, A.G., Trembovler, V., and Shohami, E. (2008). Dynamic changes in the recovery after traumatic brain injury in mice: effect of injury severity on T2-weighted MRI abnormalities, and motor and cognitive functions. J. Neurotrauma 25, 324–333.
4. Onyszchuk, G., Levine, S.M., Brooks, W.M., and Berman, N.E. (2009). Post-acute pathological changes in the thalamus and internal capsule in aged mice following controlled cortical impact injury: a magnetic resonance imaging, iron histochemical, and glial immunohistochemical study. Neurosci. Lett. 452, 204–208.
5. Mac Donald, C.L., Dikranian, K., Bayly, P., Holtzman, D., and Brody, D. (2007). Diffusion tensor imaging reliably detects experimental traumatic axonal injury and indicates approximate time of injury. J. Neurosci. 27, 11,869–11,876.
6. Foley, L.M., Hitchens, T.K., Ho, C., Janesko–Feldman, K.L., Melick, J.A., Bayir, H., and Kochanek, P.M. (2009). Magnetic resonance imaging assessment of macrophage accumulation in mouse brain after experimental traumatic brain injury. J. Neurotrauma 26, 1509–1519.
7. Bitner, B.R., Brink, D.C., Mathew, L.C., Pautler, R.G., and Robertson, C.S. (2010). Impact of arginase II on CBF in experimental cortical impact injury in mice using MRI. J. Cereb. Blood Flow Metab. 30, 1105–1109.
8. Fung, Y. (1993). *Biomechanics: Mechanical Properties of Living Tissues.* Springer-Verlag: New York.
9. Rnjak, J., Wise, S.G., Mithieux, S.M., and Weiss, A.S. (2011). Severe burn injuries and the role of elastin in the design of dermal substitutes. Tissue Eng. Part B. Rev. 17, 81–91.
10. Muthupillai, R., Lomas, D.J., Rossman, P.J., Greenleaf, J.F., Manduca, A., and Ehman, R.L. (1995). Magnetic resonance elastography by direct visualization of propagating acoustic strain waves. Science 269, 1854–1857.
11. Mariappan, Y.K., Glaser, K.J., and Ehman, R.L. (2010). Magnetic resonance elastography: a review. Clin. Anat. 23, 497–511.
12. Shire, N.J., Yin, M., Chen, J., Railkar, R.A., Fox–Bosetti, S., Johnson, S.M., Beals, C.R., Dardzinski, B.J., Sanderson, S.O., Talwalkar, J.A., and Ehman, R.L. (2011). Test–retest repeatability of MR elastography for noninvasive liver fibrosis assessment in hepatitis C. J. Magn. Reson. Imaging 34, 947–955.
13. Othman, S.F., Xu, H., Royston, T.J., and Magin, R.L. (2005). Microscopic magnetic resonance elastography (microMRE). Magn. Reson. Med. 54, 605–615.
14. Othman, S.F., Curtis, E.T., Plautz, S.A., Pannier, A.K., Butler, S.D., and Xu, H. (2012). MR elastography monitoring of tissue-engineered constructs. NMR Biomed. 25, 452–463.
15. Boulet, T., Kelso, M.L., and Othman, S.F. (2011). Microscopic magnetic resonance elastography of traumatic brain injury model. J. Neurosci. Meth. 201, 296–306.
16. Kelso, M.L., Wehner, J.M., Collins, A.C., Scheff, S.W., and Pauly, J.R. (2006). The pathophysiology of traumatic brain injury in alpha7 nicotinic cholinergic receptor knockout mice. Brain Res. 1083, 204–210.
17. Kelso, M.L., Scheff, S.W., Pauly, J.R., and Loftin, C.D. (2009). Effects of genetic deficiency of cyclooxygenase-1 or cyclooxygenase-2 on functional and histological outcomes following traumatic brain injury in mice. BMC Neurosci. 10, 108.
18. Romano, A.J., Shirron, J.J., and Bucaro, J.A. (1998). On the noninvasive determination of material parameters from a knowledge of elastic displacements theory and numerical simulation. IEEE Trans. Ultrason. Ferroelectr. Freq. Control 45, 751–759.
19. Oliphant, T.E., Manduca, A., Ehman, R.L., and Greenleaf, J.F. (2001). Complex-valued stiffness reconstruction for magnetic resonance elastography by algebraic inversion of the differential equation. Magn. Reson. Med. 45, 299–310.
20. Manduca, A., Lake, D.S., Kruse, S.A., and Ehman, R.L. (2003). Spatio-temporal directional filtering for improved inversion of MR elastography images. Med. Image Anal. 7, 465–473.
21. Donkin, J.J., and Vink, R. (2010). Mechanisms of cerebral edema in traumatic brain injury: therapeutic developments. Curr. Opin. Neurol. 23, 293–299.
22. Kuroiwa, T., Ueki, M., Ichiki, H., Kobayashi, M., Suemasu, H., Taniguchi, I., and Okeda, R. (1997). Time course of tissue elasticity and fluidity in vasogenic brain edema. Acta Neurochir. Suppl. 70, 87–90.
23. Kuroiwa, T., Yamada, I., Katsumata, N., Endo, S., and Ohno, K. (2006). Ex vivo measurement of brain tissue viscoelasticity in postischemic brain edema. Acta Neurochir. Suppl. 96, 254–257.
24. Kochanek, P.M., Marion, D.W., Zhang, W., Schiding, J.K., White, M., Palmer, A.M., Clark, R.S., O'Malley, M.E., Styren, S.D., Ho, C., et al. (1995). Severe controlled cortical impact in rats: assessment of cerebral edema, blood flow, and contusion volume. J. Neurotrauma 12, 1015–1025.
25. Baskaya, M.K., Rao, A.M., Dogan, A., Donaldson, D., and Dempsey, R.J. (1997). The biphasic opening of the blood–brain barrier in the cortex and hippocampus after traumatic brain injury in rats. Neurosci. Lett. 226, 33–36.
26. Habgood, M.D., Bye, N., Dziegielewska, K.M., Ek, C.J., Lane, M.A., Potter, A., Morganti–Kossmann, C., and Saunders, N.R. (2007).

Changes in blood–brain barrier permeability to large and small molecules following traumatic brain injury in mice. Eur. J. Neurosci. 25, 231–238.
27. Warner, L., Yin, M., Glaser, K.J., Woollard, J.A., Carrascal, C.A., Korsmo, M.J., Crane, J.A., Ehman, R.L., and Lerman, L.O. (2011). Noninvasive In vivo assessment of renal tissue elasticity during graded renal ischemia using MR elastography. Invest. Radiol. 46, 509–514.
28. Engel, D.C., Mies, G., Terpolilli, N.A., Trabold, R., Loch, A., De Zeeuw, C.I., Weber, J.T., Maas, A.I., and Plesnila, N. (2008). Changes of cerebral blood flow during the secondary expansion of a cortical contusion assessed by 14C-iodoantipyrine autoradiography in mice using a non-invasive protocol. J. Neurotrauma 25, 739–753.
29. Schwarzmaier, S.M., Kim, S.W., Trabold, R., and Plesnila, N. (2010). Temporal profile of thrombogenesis in the cerebral microcirculation after traumatic brain injury in mice. J. Neurotrauma 27, 121–130.
30. Schuhmann, M.U., Stiller, D., Skardelly, M., Mokktarzadeh, M., Thomas, S., Brinker, T., and Samii, M. (2002). Determination of contusion and oedema volume by MRI corresponds to changes of brain water content following controlled cortical impact injury. Acta Neurochir. Suppl. 81, 213–215.
31. Baldwin, S.A., Fugaccia, I., Brown, D.R., Brown, L.V., and Scheff, S.W. (1996). Blood–brain barrier breach following cortical contusion in the rat. J. Neurosurg. 85, 476–481.
32. Fukuda, A.M., Pop, V., Spagnoli, D., Ashwal, S., Obenaus, A., and Badaut, J. (2012). Delayed increase of astrocytic aquaporin 4 after juvenile traumatic brain injury: possible role in edema resolution? Neuroscience 222, 366–378.
33. Atay, S.M., Kroenke, C.D., Sabet, A., and Bayly, P.V. (2008). Measurement of the dynamic shear modulus of mouse brain tissue in vivo by magnetic resonance elastography. J. Biomech. Eng. 130, 021013.
34. Clayton, E.H., Garbow, J.R., and Bayly, P.V. (2011). Frequency-dependent viscoelastic parameters of mouse brain tissue estimated by MR elastography. Phys. Med. Biol. 56, 2391–2406.
35. Murphy, M.C., Curran, G.L., Glaser, K.J., Rossman, P.J., Huston, J., 3rd, Poduslo, J.F., Jack, C.R., Jr., Felmlee, J.P., and Ehman, R.L. (2012). Magnetic resonance elastography of the brain in a mouse model of Alzheimer's disease: initial results. Magn. Reson. Imaging. 30, 535–539.
36. Elkin, B.S., Azeloglu, E.U., Costa, K.D., and Morrison, B., 3rd. (2007). Mechanical heterogeneity of the rat hippocampus measured by atomic force microscope indentation. J. Neurotrauma 24, 812–822.
37. Christ, A.F., Franze, K., Gautier, H., Moshayedi, P., Fawcett, J., Franklin, R.J., Karadottir, R.T., and Guck, J. (2010). Mechanical difference between white and gray matter in the rat cerebellum measured by scanning force microscopy. J. Biomech. 43, 2986–2992.
38. Elkin, B.S., Ilankovan, A., and Morrison, B., 3rd. (2010). Age-dependent regional mechanical properties of the rat hippocampus and cortex. J. Biomech. Eng. 132, 011010.
39. van Dommelen, J.A., van der Sande, T.P., Hrapko, M., and Peters, G.W. (2010). Mechanical properties of brain tissue by indentation: interregional variation. J. Mech. Behav. Biomed. Mater. 3, 158–166.
40. Prevost, T.P., Jin, G., de Moya, M.A., Alam, H.B., Suresh, S., and Socrate, S. (2011). Dynamic mechanical response of brain tissue in indentation in vivo, in situ and in vitro. Acta Biomater. 7, 4090–4101.
41. Johnson, C.L., McGarry, M.D., Van Houten, E.E., Weaver, J.B., Paulsen, K.D., Sutton, B.P., and Georgiadis, J.G. (2012). Magnetic resonance elastography of the brain using multishot spiral readouts with self-navigated motion correction. Magn. Reson. Med. Epub ahead of print.
42. Hamhaber, U., Klatt, D., Papazoglou, S., Hollmann, M., Stadler, J., Sack, I., Bernarding, J., and Braun, J. (2010). In vivo magnetic resonance elastography of human brain at 7 T and 1.5 T. J. Magn. Reson. Imaging 32, 577–583.

Address correspondence to:
Shadi F. Othman, PhD
Translational and Regenerative Medicine (TREM)
Imaging Laboratory
249 L.W. Chase Hall
University of Nebraska-Lincoln
Lincoln, NE 68583

E-mail: sothman2@unl.edu